Track density imaging (TDI): validation of super-resolution property

F. Calamante[1,2], J-D. Tournier[1,2], R. M. Heidemann[3], A. Anwander[3], G. D. Jackson[1,2], and A. Connelly[1,2]
[1]Brain Research Institute, Florey Neuroscience Institutes, Heidelberg West, Victoria, Australia, [2]Department of Medicine, University of Melbourne, Melbourne, Victoria, Australia, [3]Max Planck Institute for Human Cognitive and Brain Sciences, Leipzig, Germany

Introduction: *Super-resolution track-density imaging* (TDI) has been recently introduced as a means to achieve high-quality white matter images, with very high spatial-resolution and anatomical contrast (1). This method achieves super-resolution by using the long-range information contained in the diffusion MRI fibre-tracks; the density of a large number of streamlines provides intra-voxel information to generate an image with higher resolution than that of the acquired source diffusion-weighted imaging (DWI) data (1). Super-resolution MRI methods have been used previously, including controversial applications to DWI (2). All previous methods are based on the more commonly used super-resolution principle: combining images acquired with relative sub-voxel shifts, which it is generally accepted can only achieve super-resolution in the slice direction (3). This limitation does not apply to super-resolution TDI since it relies on a different principle. As with any new technique offering super-resolution, the question arises as to the validity of the extra information generated: are the structures that appear following the super-resolution processing an artefact of the process itself? We validate here the super-resolution property of the TDI method by using *in vivo* 7T DWI data, and *in silico* DWI data from a well-characterised numerical phantom (4).

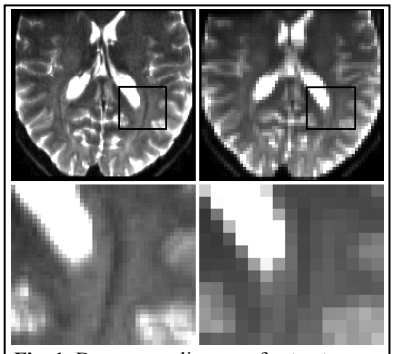

Fig. 1: Down-sampling step for *in vivo* data. Top-left: gold-standard (*GS*) image (0.8mm isotropic). Top-right: lower resolution (*LR*) down-sampled image (2.4 mm isotropic). Bottom: zoomed regions.

Methods: *In vivo data:* High-resolution DWI data were acquired from a healthy volunteer at 7T (Siemens) using the previously published ZOOPPA acquisition protocol (5) (1 mm isotropic resolution, b=1000s/mm^2, 60 DW-directions, 6 repeats, acquisition time = 69min). For anatomical reference, a conventional T1-weighted image (0.8mm isotropic) was also acquired. *In vivo data pre-processing:* T1-weighted data were co-registered to Talairach space, and DWI data were motion-corrected and registered to T1 data. Data were interpolated to the new reference frame with 0.8mm isotropic resolution; this 0.8mm DWI data-set will be our *reference* data-set and referred to as the 'gold-standard' (*GS*). This GS data-set was down-sampled by a factor of 3 to *simulate* a DWI data-set that would have been acquired at a lower 2.4 mm isotropic resolution (Fig. 1); this 2.4 mm data-set will be referred to as the 'low resolution' (*LR*) data. *In silico data:* The numerical *Phantom A* from the *NFG* software package (4,6) was used for this study, and DWI data were simulated with b=3000s/mm^2, 60 DW-directions, 2mm voxel-size, and SNR=17.

Fibre-tracking: Whole brain (or phantom) fibre-tracking was performed using in-house software based on *MRtrix* (6), including CSD (7) to model multiple fibre orientations, and probabilistic tracking using 2nd order integration over fibre orientation distributions (iFOD2) (8): 1mm step-size, 3 FOD samples/step, termination criteria: exit the brain/phantom or when FOD amplitude < 0.1. Two million tracks were generated (randomly seeded) for each data-set.

Track-density imaging: TDI maps were generated by counting the number of tracks in each grid-element (Note: grid-elements can be smaller than voxel-size of source data (1)). For the *LR in vivo* data-set, a 0.8mm isotropic grid was used with super-resolution TDI (*super-TDI*$_{LR}$ map) (i.e. 2.4mm source *LR* DWI data super-resolved to 0.8mm TDI map); for comparison, a TDI map without super-resolution (2.4mm grid) was also created (*TDI*$_{LR}$). For the *GS in vivo* data-set, the same 0.8mm grid was used for TDI *without* super-resolution (*TDI*$_{GS}$ map). Therefore, *super-TDI*$_{LR}$ and *TDI*$_{GS}$ have the same resolution, but *only* the *super-TDI*$_{LR}$ map was constructed using super-resolution; by comparing these maps, the effect of super-resolution can be evaluated. A similar analysis was performed for the *in silico* data (with 0.2mm grid to generate super-resolution TDI, and 2mm grid without super-resolution); for the phantom, the gold-standard is given by the known simulated structure (4). Due to the lack of TDI contrast in the phantom, the directionally-encoded colour (DEC) version of the TDI maps (1) was used.

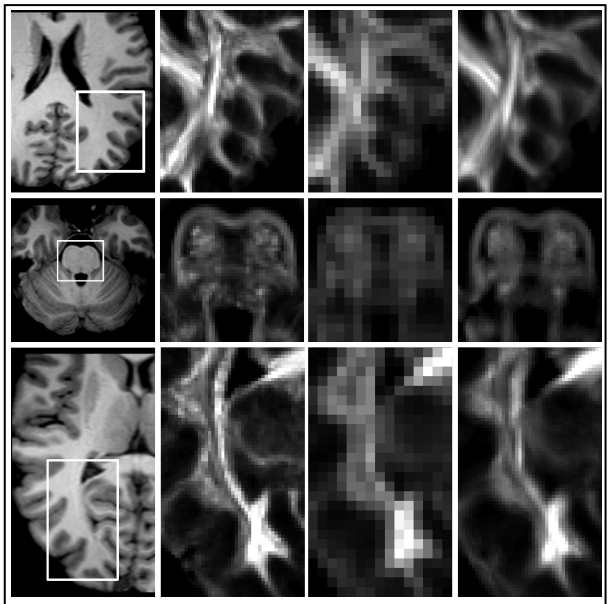

Fig. 2: Structures identified by super-resolution step at 3 axial levels (rows). Left: T1-weighted image with zoomed region. Second column: gold-standard TDI maps (*TDI*$_{GS}$) with 0.8 mm isotropic resolution. Third-column: low-resolution TDI map (*TDI*$_{LR}$) with 2.4 mm resolution. Right: super-resolution TDI map of the low-resolution data (*superTDI*$_{LR}$) with 0.8 mm resolution.

Results: As can be seen in the *in vivo* (Fig. 2) and *in silico* examples (Fig. 3), the structures generated by the super-resolution method are consistent with those observed in the gold-standard TDI maps. Note also that these structures are not apparent in the low resolution maps, emphasising the power of the super-resolution TDI. It should be noted that short fibre-bundles tend to have fewer tracks (less seed-points), which leads to reduced TDI intensity (e.g. see relatively low intensity of peripheral short bundles in the phantom).

Discussion: This study validates the super-resolution property of the TDI method. Both the *in vivo* and *in silico* data show that the structures that could be identified in the TDI map *only* after using super-resolution were consistent with the corresponding structures identified in the reference maps. This supports the claim that the structures generated by the super-resolution step are accurate and not an artefact of the super-resolution process itself. This provides further evidence for the important potential role of the super-resolution TDI methodology in neuroscience.

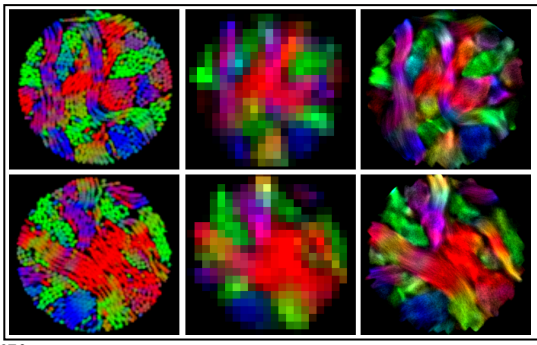

Fig. 3: Directionally-encoded color (DEC) TDI maps for two phantom slices. Left: simulated structures. Middle: DEC TDI map created without super-resolution (2mm isotropic). Right: DEC TDI map with super-resolution (0.2mm grid). Color-coding indicates main local orientation.

References: (1) Calamante F, et al. *NeuroImage* 2010;53:1233. (2) Scheffler K. *MRM* 2002;48:408. (3) Greenspan H, et al. *MRI* 2002;20:437. (4) Close TG, et al. *NeuroImage* 2009;47:1288. (5) Heidemann RM, et al. *ISMRM* 2010;18:1610. (6) http://www.brain.org.au/software/ (7) Tournier JD et al. *NeuroImage* 2007;35:1459. (8) Tournier JD et al. *ISMRM* 2010;18:1670.